An extension of Osher's Riemann solver for chemical and vibrational non equilibrium gas flows

Remi Abgrall, Loula Fatima Fezoui, Jean Talandier

UNITÉ DE RECHERCHE
INRIA-SOPHIA ANTIPOLIS

Institut National
de Recherche
en Informatique
et en Automatique

Domaine de Voluceau
Rocquencourt
B.P.105
78153 Le Chesnay Cedex
France
Tél.:(1) 39 63 55 11

Rapports de Recherche

N° 1221

Programme 7
Calcul Scientifique,
Logiciels Numériques et Ingénierie Assistée

AN EXTENSION OF OSHER'S RIEMANN SOLVER FOR CHEMICAL AND VIBRATIONAL NON EQUILIBRIUM GAS FLOWS

Rémi ABGRALL
Loula FEZOUI
Jean TALANDIER

Mai 1990

RR.1221

Programme 7

AN EXTENSION OF OSHER'S RIEMANN SOLVER

FOR CHEMICAL AND VIBRATIONAL NON EQUILIBRIUM GAS FLOWS

Rémi ABGRALL, , Loula FEZOUI, Jean TALANDIER

1990

Résumé

Dans ce rapport, nous définissons une extension du solveur de Riemann adaptée au calcul d'écoulements de gaz réels hors équilibre chimique et vibrationel. Nous illustrons les capacités et la robustesse de ce nouveau solveur sur des exemples mono- et bidimensionels. Nous montrons sur ces exemples numériques que les principales propriétés du solveur d'Osher sont encore vraies ; en particulier, il n'est pas nécessaire d'ajouter une quelconque correction entropique pour le calcul d'écoulements hypersonique.

Abstract

In this paper, we define an extension of Osher's Riemann solver adapted to chemically and vibrationally nonequilibrium flows. Some of its properties are discussed. We give 1D and 2D applications to illustrate the robustness and capability of this new solver. We show on numerical examples that the main properties of the Osher's solver are preserved ; in particular no entropy fix is needed even for hypersonics applications.

AN EXTENSION OF OSHER'S RIEMANN SOLVER FOR CHEMICAL AND VIBRATIONAL NON EQUILIBRIUM GAS FLOWS

EXTENSION DU SOLVEUR DE RIEMANN D'OSHER POUR LES ECOULEMENTS HORS EQUILIBRE CHIMIQUE ET VIBRATIONNEL

Rémi ABGRALL, , Loula FEZOUI, Jean TALANDIER

INRIA
Centre de Sophia Antipolis
2004, route des Lucioles
06560 VALBONNE
FRANCE

Notations

- $\mathcal{R}$ is the universal constant of perfect gases
- m_i molar weight of species i
- $R_i = \frac{\mathcal{R}}{m_i}$
- c_{v_i} and c_{p_i} are the specific heats of species i.
- $\gamma_i = \frac{c_{p_i}}{c_{v_i}}$
- $\kappa_i = \gamma_i - 1$
- T is the temperature of the flow
- ρ_i is the density of species i
- ρ is the total density, $\rho = \sum_{i=1}^{ns} \rho_i$
- $Y_i = \frac{\rho_i}{\rho}$ is the mass fraction of species i
- h_i^0 is the enthalpy of formation of species i
- θ_i is a typical value of the vibrational temperature of the molecules of species i
- p is the pressure
- u is the velocity, $m = \rho u$ is the momentum
- e is the total energy per unit volume
- ϵ is the specific energy per unit volume
- e_{vib}^i specific vibrational energy of species i
- $H = \frac{e+p}{\rho}$ is the specific enthalpy

Chapter 1

Introduction

During the past few years, because of the existence of many transatmospheric vehicles projects both in the US and Europe, many researchers have been working on the numerical simulation of hypersonic flows.

Among the various methods proposed in literature, upwind methods have encountered great success in the study of transsonic and supersonic flows. A very natural wish is to extend them to hypersonic purposes. Besides the stiffness of the problem (very strong shock or expansion waves wave develop), new phenomena occur due to the high level of temperature encountered in such gases ; chemistry, vibrational relaxation and possibly ionisation have to be taken into account. All classical Riemann solvers have been derived with the perfect gas law assumption and then have to be adapted to real gases.

Many solutions have been presented to generalize Van Leer's solver (see [6,16,12,17], for example) or Roe's (see [6,23,3,11,17]) in thermal and chemical equilibrium. More recently, the same work has been done for non equilibrium chemistry and non equilibrium vibrational relaxation (see [4,5,25,14] for example).

In classical applications, one of the most interesting solver is Osher's [22]. The principle of Osher's Riemann solver is to solve the Riemann problem by connecting the two states in consideration with three sub pathes. Each of them consists in a compression or an expansion wave and a contact discontinuity and then, one have to average the flux on this multivalued path. We will precisely recall how to build this numerical flux in Section 3.2. Two versions of Osher's solver are used depending on the path chosen in its definition.

The main properties of this numerical flux are :1) robustness, 2) smoothness at transition points, 3) satisfy an entropy inequality and 4) stationary and sharp contact discontinuity and shocks. The point 3) has been shown at least for one version of the scheme [22] but shown experimentally to be true for the other one. This scheme uses informations related to the Riemann problem. Its utilization for more general cases than that of perfect gases needs further work.

The extension of this particular Riemann solver have been first (to our knowledge) generalized for real gases by Abgrall et al. [19] then by Dubois [10] and very recently by Suresh et al. [2]. The difference between these versions mainly lies in the way of calculating the ends of the connecting pathes and the sonic points and how the true pathes are approximated. The version presented in [19] is simpler than Suresh's and experimentally respects condition 1)-4) but the latter one, depending on what computational effort is requested, may be more accurate and leads to variations. In Dubois's

version, one tries to tabulate the Riemann invariant of the problem.

In the present report, we use basically the same approach than in [19] but with some novelties. From the expression of the Jacobian matrix of the Euler fluxes, we first study the behaviour of its eigenvalues. Then we describe the Riemann invariants of the system and propose and discuss a method for their integration. Several test cases both 1-D and 2-D are considered to show the efficiency and the robustness of the method. Particular emphasis is put on the entropy property of this solver.

Chapter 2

Equation of state, physical model, eigenvalues and eigenvectors

2.1 Equation of state

We consider a mixture of ns perfect gases. The internal energy of a given species is :

$$\epsilon_i = \rho_i c_{v_i} T + \rho_i {h_i}^0 + \rho_i e^i_{vib}$$

where T is the translational temperature, ${h_i}^0$ is the enthalpy of formation of this particular species at a given reference temperature and e^i_{vib} is the specific vibrational of species i (this term disappears for the monoatomic species).

We assume that some of the diatomic species may not be at thermal equilibrium with the translational temperature T. Let T_i be the vibrational temperature of species i. We will assume that the vibrational energy ${E^{vib}}_i$ is related to T_i and ρ_i by :

$$E^{vib}_i = \rho_i \frac{R_i \theta_i}{exp(\frac{\theta_i}{T_i}) - 1} = \rho_i e^{vib}_i \tag{2.1}$$

If species i is at thermal equilibrium, $T_i = T$ in equation(2.1)

The internal energy ϵ is the sum of each internal energy :

$$\epsilon = \sum_{i=1}^{ns} \rho_i c_{v_i} T + \sum_{i=1}^{ns} \rho_i {h_i}^0 + \sum_{i=1}^{nv_1} {E^{vib}}_i + \sum_{i=nv_1+1}^{nv} \rho_i e^{vib}_i \tag{2.2}$$

In equation (2.2), nv is the number of diatomic species ; they are assumed to be the nv first ones among which the nv_1 first diatomic species are not at thermal equilibrium.

The pressure is given by Dalton's law :

$$p = \sum_{i=1}^{ns} \rho_i c_{v_i} \kappa_i T = \rho c_v \kappa T, \tag{2.3}$$

where $c_v = \sum_{i=1}^{ns} Y_i c_{v_i}$ and $\kappa = \frac{\sum_{i=1}^{ns} Y_i c_{v_i} \kappa_i}{\sum_{i=1}^{ns} Y_i c_{v_i}}$.

2.2 Euler equations

We consider thermal and vibrational non equilibrium. The independent variables which describe the system are the partial densities, momentum ρu, total energy $e = \epsilon + \frac{1}{2}\rho u^2$ and vibrational energies. In 1 D, they obey the Euler equation with possibly source terms if we consider chemistry and vibrational relaxation.

$$\frac{\partial W}{\partial t} + \frac{\partial F}{\partial x} = \Omega$$

with

$$W = \begin{pmatrix} \rho_1 \\ \dots \\ \rho_{ns} \\ \rho u \\ e \\ E_1^{vib} \\ \dots \\ E_{nv_1}^{vib} \end{pmatrix} \quad F(W) = \begin{pmatrix} \rho_1 u \\ \dots \\ \rho_{ns} u \\ \rho u^2 + p \\ u(e+p) \\ E_1^{vib} u \\ \dots \\ E_{nv_1}^{vib} u \end{pmatrix} \quad \Omega = \begin{pmatrix} \Omega_1^{chim} \\ \dots \\ \Omega_{ns}^{chim} \\ 0 \\ 0 \\ \Omega_1^{vib} \\ \dots \\ \Omega_{nv_1}^{vib} \end{pmatrix} \tag{2.4}$$

2.3 Chemical model

In the following, we assume a mixture of five species which compose air, namely : O, N, NO, O_2 and N_2.

We first describe the expression of the dissociation and recombination model and then the vibrational relaxation one.

The dissociation and recombination model is Park's [8] in which we retain the 17 chemical reactions which involve O, N, NO, O_2 and N_2. For sake of simplicity, thought this assumption may be unphysical, we assume no coupling between vibration and chemistry. Consequently, the forward and backward constants in Park's model are obtained with the translational temperature only. The dissociation and recombination reactions source term for species i is denoted Ω_i^{chim}.

For the vibrational relaxation, we assume the Landau-Teller model [24]. The precise values of the characteristic times involved in the definition of τ_i can be found in the same reference. The source term for vibrational relaxation takes the form (for a given diatomic species i) :

$$\Omega_i^{vib} = \Omega_i^{chim} \frac{E_i^{vib}}{\rho_i} + \frac{E_i^{vib} - E_i^{vib}}{\tau_i} \tag{2.5}$$

in equation (2.5), E_{vib}^{s} stands for the vibrational energy at thermal equilibrium of species s.

2.3.1 Jacobian matrix

We immediately get

$$\frac{\partial F(W)}{\partial W} = \begin{pmatrix} (1-Y_1)u & \cdots & -Y_1 u & Y_1 & 0 & 0 & \cdots & 0 \\ \vdots & \vdots & \vdots & \vdots & \vdots & \vdots & \vdots & \vdots \\ -Y_{ns}u & \cdots & (1-Y_{ns})u & Y_{ns} & 0 & 0 & \cdots & 0 \\ -u^2+p_{\rho_1} & \cdots & -u^2+p_{\rho_{ns}} & 2u+p_{\rho u} & p_E & p_{E_1{}^{vib}} & \cdots & p_{E_{nv_1}{}^{vib}} \\ (-H+p_{\rho_1})u & \cdots & (-H+p_{\rho_{ns}})u & H+p_{\rho u}u & (1+p_E)u & up_{E_1{}^{vib}} & \cdots & up_{E_{nv_1}{}^{vib}} \\ -u\dfrac{E_1{}^{vib}}{\rho} & \cdots & -u\dfrac{E_1{}^{vib}}{\rho} & \dfrac{E_1{}^{vib}}{\rho} & 0 & u & \cdots & 0 \\ \vdots & \vdots & \vdots & \vdots & \vdots & \vdots & \vdots & \\ \vdots & & & & & & & \\ -u\dfrac{E_{nv_1}{}^{vib}}{\rho} & \cdots & -u\dfrac{E_{nv_1}{}^{vib}}{\rho} & \dfrac{E_{nv_1}{}^{vib}}{\rho} & 0 & 0 & \cdots & u \end{pmatrix} \tag{2.6}$$

where p_z stands for the partial derivative of p towards any conservative variable $z = W_k$. In equation (2.6), we have set :

$$p_{\rho_i} = \chi_i + \kappa_{so}\frac{u^2}{2} \qquad p_{\rho u} = -\kappa_{so}u \qquad p_E = \kappa_{so} \qquad p_{E_i{}^{vib}} = -\kappa_{so}$$

with :

$$\kappa_{so} = \frac{\sum_{i=1,ns} Y_i R_i}{\sum_{i=1,ns} Y_i c_{vi} + \sum_{i=nv_1+1,nv} Y_i \dfrac{de_{vib}{}^i}{dT}}$$

and

$$\chi_i = c_{vi}(\kappa_i - \kappa_{so})T - \kappa_{so}\left(h_i{}^0 + \epsilon_i e_{vib}{}^i\right)$$

In the latter expression, ϵ_i has value 1 if species i is diatomic and at thermal equilibrium and 0 else.

It is straightforward to check that the fluxes F are homogeneous of degre one and that matrix $\frac{\partial F(W)}{\partial W}$ is diagonalizable and has real eigenvalues.

Right eigenvectors : The following matrix R describes its eigenvectors, the lth column of R is the lth eigenvector of $\frac{\partial F(W)}{\partial W}$:

$$R = \begin{pmatrix} 1 & 0 & \cdots & 0 & 0 & \cdots & 0 & Y_1 & Y_1 \\ 0 & 1 & \cdots & 0 & 0 & \cdots & 0 & Y_2 & Y_2 \\ \vdots & \vdots & \vdots & \vdots & \vdots & \vdots & \vdots & \vdots & \vdots \\ 0 & 0 & \cdots & 1 & 0 & \cdots & 0 & Y_{ns} & Y_{ns} \\ u & u & \cdots & u & 1 & \cdots & 1 & u-a & u+a \\ \dfrac{u^2}{2}-\dfrac{\chi_1}{\kappa} & \dfrac{u^2}{2}-\dfrac{\chi_2}{\kappa} & \cdots & \dfrac{u^2}{2}-\dfrac{\chi_{ns}}{\kappa} & 1 & \cdots & 1 & H-ua & H+ua \\ 0 & 0 & \cdots & 0 & 1 & \cdots & 0 & \dfrac{E_1{}^{vib}}{\rho} & \dfrac{E_1{}^{vib}}{\rho} \\ \vdots & \vdots & \vdots & \vdots & \vdots & \vdots & \vdots & \vdots & \vdots \\ 0 & 0 & \cdots & 0 & 0 & \cdots & 1 & \dfrac{E_{ns}{}^{vib}}{\rho} & \dfrac{E_{ns}{}^{vib}}{\rho} \end{pmatrix}$$

In matrix R, the $ns+nv_1$ first columns are associated to the eigenvalue $\lambda_1 = u$, the next column to eigenvalue $\lambda_2 = u + a$ and the last one to $\lambda_3 = u + a$ where a is the speed of sound the square of which is :

$$a^2 = \sum_{i=1,ns} \chi_i Y_i + \kappa_{so} \left[H - \sum_{nv_1+1}^{ns} {e_{vib}}^i - \frac{u^2}{2} \right] \tag{2.7}$$

Let us notice that the square of the speed of sound can also be written as :

$$a^2 = \gamma_{so} \frac{p}{\rho}. \tag{2.8}$$

with $\gamma_{so} = \kappa_{so} + 1$. It is straightforward to check that the eigenvectors associated to λ_1 are linearly degenerate while those associated with the other eigenvalues are genuinely non linear. More precisely, we have :

- For $i = 1, ns + nv_1$, $\nabla \lambda_i . R_i = 0$
- $\nabla(u - a).R_{ns+nv_1+1} = -(\gamma_{so} + 1)\frac{a}{2\rho} < 0$
- $\nabla(u + a).R_{ns+nv_1+2} = (\gamma_{so} + 1)\frac{a}{2\rho} > 0$

Left eigenvectors : One can easily get the left eigenvectors of the Jacobian matrix : they are linear forms which expression in term of any vector $V = (V_1, \cdots, V_{ns+nv_1+2})^T$ are :

- for $i = 1, ns$,

$$l_i(V) = V_i - \frac{Y_i \kappa_{so}}{a^2} \left[V_{ns+2} - \sum_{l=ns+3}^{ns+nv_1+2} V_l - uV_{ns+1} + \frac{u^2}{2} \sum_{l=1,ns} V_l + \sum_{l=1,ns} \frac{\chi_l V_l}{\kappa_{so}} \right]$$

- for $i = ns + 1, ns + 1 + nv_1$,

$$l_i(V) = V_i - \frac{{E_{vib}}^i}{\rho} \frac{\kappa_{so}}{a^2} \left[V_{ns+2} - \sum_{l=ns+3}^{ns+nv_1+2} V_l - uV_{ns+1} + \frac{u^2}{2} \sum_{l=1,ns} V_l + \sum_{l=1,ns} \frac{\chi_l V_l}{\kappa_{so}} \right]$$

- for $i = ns + 2 + nv_1, ns + 3 + nv_1$,

$$l_i(V) = \frac{1}{2a} \left[V_{ns+1} - u \sum_{l=1,ns} V_l \right] \pm \frac{\kappa_{so}}{a^2} \left[V_{ns+2} - \sum_{l=ns+3}^{ns+nv_1+2} V_l - uV_{ns+1} + \frac{u^2}{2} \sum_{l=1,ns} V_l + \sum_{l=1,ns} \frac{\chi_l V_l}{\kappa_{so}} \right]$$

2.4 Riemann Invariants

In this section, we intend to derive the differential equations satisfied by the Riemann invariants of the PDE system considered now without the source terms (ie $\Omega = 0$) :

$$\frac{\partial W}{\partial t} + \frac{\partial F(W)}{\partial x} = 0$$

where W and $F(W)$ have been defined in equation (2.4).

Let us consider an eigenvalue of $\frac{\partial F}{\partial W}$, say λ_k . A Riemann invariant associated to the eigenvalue λ_k is a function Φ^k of W such that for any eigenvector R_l which does not belong to the kernel of $\frac{\partial F(W)}{\partial W} - \lambda_k Id$,

$$\nabla_W \Phi^k \, . \, R_l = 0$$

The solutions of these sets of equation can be obtained in the phase space considering the paths $s \longmapsto W(s)$ such that $\frac{dW}{ds}$ is belongs to the eigenvector space associated to eigenvalue λ.

If we use the right eigenvectors defined above, we may see that the Riemann invariants, in the problem considered here, are solutions of the following differential equations :

- Eigenvalue $\lambda_1 = u$:

$$\rho \frac{du}{ds} \pm \frac{1}{a} \frac{dp}{ds} = 0 \tag{2.9}$$

- Eigenvalue $\lambda_2 = u + a$:

$$\frac{d\rho_i}{ds} - \frac{Y_i}{a^2} \frac{dp}{ds} \quad i = 1, ns \tag{2.10}$$

$$\frac{dY_i e^i_{vib}}{ds} - \frac{Y_i e^i_{vib}}{a^2} \frac{dp}{ds} \quad i = 1, nv_1 \tag{2.11}$$

$$\rho \frac{du}{d\rho} + \frac{1}{a} \frac{dp}{ds} = 0 \tag{2.12}$$

- Eigenvalue $\lambda_3 = u - a$:

$$\frac{d\rho_i}{ds} - \frac{Y_i}{a^2} \frac{dp}{ds} \quad i = 1, ns \tag{2.13}$$

$$\frac{dY_i e^i_{vib}}{ds} - \frac{Y_i e^i_{vib}}{a^2} \frac{dp}{ds} \quad i = 1, nv_1 \tag{2.14}$$

$$\rho \frac{du}{d\rho} - \frac{1}{a} \frac{dp}{ds} = 0 \tag{2.15}$$

We can see that there are 2 equations for λ_1 and $ns + nv_1 + 1$ equations for λ_2 and λ_3.

Discussion

These differential equations may be difficult to solve (and in general impossible to solve by hand) because γ_{so} depends, in general, both form the temperature and the mass fraction. Nevertheless, it is possible to make some general comments :

1. Case of the linearly degenerate fields : it is obvious, from equations (2.9) that the pressure p and the velocity u remain constant in a wave associated to λ_1

2. Case of the genuinely nonlinear fields. If one sums up equations (2.10), one gets :

$$\frac{d\rho}{ds} = \frac{1}{a^2}\frac{dp}{ds}$$

Since $Y_i = \frac{\rho_i}{\rho}$, we can deduce that the mass fractions Y_i remains constants in sonic wave.

The same is true for the specific vibrational energy $\frac{E_{vib}^i}{\rho} = Y_i e_{vib}^i$.

The other equations are considered in Section 3.3.

Chapter 3

An extension of Osher's Riemann solver

This section is divided into three parts : in the first one, we recall the definition of Osher's Riemann solver in the most general case, then we derive an approximation of it in the case we are looking at here and lastly, we comment some of its properties.

3.1 Definition of Osher's Riemann solver

We will recall some details of Osher-Solomon's paper [22] and Osher-Chakravarthy's [21].

Let us give an hyperbolic partial differential system of equations in conservative form :

$$\frac{\partial W}{\partial t} + \frac{\partial F}{\partial x}(W) = 0.$$

Osher's approximate Riemann solver is defined by :

$$\mathcal{F}(U,V) = \frac{1}{2}\left[F(U) + F(V) - \int_{\Gamma} \mid A(W) \mid dW\right] \tag{3.1}$$

where A is the Jacobian matrix of F, $\mid A \mid$ admits the same eigenvectors as A but its eigenvalues are the absolute values of that of A and the integral path Γ connects the two states U and V.

In references [22,21], the path Γ is always tangent to the right eigenspaces of matrix A and is the reunion of three subpathes, Γ_1, Γ_2, Γ_3 where Γ_i is tangent to the eigenspace defined by λ_i. Different way of ordering the eigenvalues of A can be considered. The optimum choices seem to be the "natural" order $(u-a, u, u+a)$ or the inverse order $(u+a, u, u-a)$. In [22], it was shown that the definition of Osher's solver combined to the "reverse" order leads to a numerical flux which respect an entropy inequality for the semi-discrete scheme. To our knowledge, nothing has been done for the "natural" order.

In the following, we use the reverse order but all what we say can easily be transposed to the other choice of parametrization.

3.2 Expression of the numerical flux

One introduce intermediate states which are the end of pathes Γ_1, Γ_2 and Γ_3. They are (see Figure 3.1) :

- $U_{1/3} = \Gamma_2 \cap \Gamma_1$
- $U_{2/3} = \Gamma_3 \cap \Gamma_1$

The definition of these intermediate states is precised in Section 3.4. Since the eigenvectors associated to $u \pm a$ are genuinely nonlinear, the eigenvalues $u \pm a$ may change their sign at most once. These points, if they exist, are called sonic points and be denoted by $\overline{U_{1/3}}$ (respectively $\overline{U_{2/3}}$) in the path Γ_2 (respectively Γ_3).

- Case of the genuinely nonlinear vectors :

$$\begin{aligned} \int_{\Gamma_1} \mid A \mid dW &= \int_U^{\overline{U_{1/3}}} A^+ dW - \int_{\overline{U_{1/3}}}^{U_{1/3}} A^- dW \\ &= sign(\lambda_1(U))\ [F(\overline{U_{1/3}}) - F(U)] + \\ &\quad sign(\lambda_1(\overline{U_{1/3}}))\ [F(U_{1/3}) - F(\overline{U_{1/3}}] \end{aligned} \tag{3.2}$$

  The last equality (3.2) is true because the flux is homogeneous of degree one. The same things can be done along path Γ_3.

- Case of the linearly degenerate fields : we have shown in Section 2.4 that the velocity remains constant in an u-wave. Since the fluxes are homogeneous of degree one, we get :

$$\int_{\Gamma_2} \mid A \mid dW = sign(U_{1/3})[F(U_{2/3}) - F(U_{1/3})] \tag{3.3}$$

3.3 Approximate Riemann invariants

The pathes are determined using the Riemann invariants since the invariants associated with a given wave remain, by definition, constant on that wave. In the perfect gas case for example, it is very easy to determine exact formulaes of the Riemann invariant, so the intermediate states are trivial to compute. Here, this is not true for the genuinely nonlinear waves.

To begin with, let us recall the equations the invariants satisfy :

- The mass fractions Y_i and the specific vibrational energies $\frac{E_i^{vib}}{\rho}$ for $i = 1, nv_1$ remain constant.
- We have :

$$\frac{d\rho}{ds} - \frac{1}{a^2}\frac{dp}{ds} = 0 \tag{3.4}$$

$$\rho\frac{du}{ds} \pm \frac{1}{a}\frac{dp}{ds} = 0 \tag{3.5}$$

On one hand, because of the expression of the speed of sound (2.7), Equation (3.4) is equivalent to :

$$dp = \left\{ \sum_{i=1,ns} \chi_i Y_i + \kappa_{s\rho} \left[H - \sum_{nv_1+1}^{nv} \frac{E_i^{vib}}{\rho} - \frac{u^2}{2} \right] \right\} d\rho \tag{3.6}$$

We also have, by definition,

$$dp = \sum_{i=1}^{n.s} \chi_i d\rho_i + \kappa_{so} d\epsilon \tag{3.7}$$

Since the mass fractions are constant, equations (3.5)-(3.7) leads to :

$$\frac{d\epsilon'}{\epsilon'} = (1 + \frac{p}{\epsilon'})\frac{d\rho}{\rho} \tag{3.8}$$

In equation 3.8, we have set :

$$\epsilon' = \epsilon - \sum_{i=nv_1+1}^{nv} E^i_{vib} \tag{3.9}$$

On the other hand, because of equation (2.8), equation (3.4) leads directly to :

$$\frac{dp}{p} = \gamma_{so} \frac{d\rho}{\rho} \tag{3.10}$$

To obtain easily the internal energy and the pressure from equations (3.8), 3.9 and (3.10), one have to make two assumptions we discuss below :

- *Assumption No 1 :* $\gamma_{eq} = 1 + \frac{p}{\epsilon}$ is approximately constant in an expansion or a compression wave
- *Assumption No 2 :* The same is true for γ_{so}.

In general, these assumptions may be completely wrong. Nevertheless, to our experience (shock tubes, blunt bodies and nozzle), they are not restrictive. Let us also notice that γ_{eq} and γ_{so} are in general function of the temperature T and the mass fractions. Since the mass fractions remain constant in an expansion/compression wave, both "gammas" depend only on the temperature. Moreover, if there is no vibrational terms or if there is as many vibrational temperature as diatomic species, then both gamma are equal and constant. So, we turn back to the mixture of perfect gases case.

If both assumptions are done, the integration of equation (3.8) and (3.10) is trivial and leads to :

$$\frac{\epsilon}{\epsilon_0} = \left(\frac{\rho}{\rho_0}\right)^{\gamma_{eq}} \tag{3.11}$$

$$\frac{p}{p_0} = \left(\frac{\rho}{\rho_0}\right)^{\gamma_{so}} \tag{3.12}$$

The integration of equation (3.5) is easy :

$$u \pm \frac{2}{\gamma_{so} - 1} a = cte \tag{3.13}$$

The approximate Riemann invariant are summarized in Table 3.3

$u-a$	u	$u+a$
$\Psi_1^1 = \frac{p}{\rho^{\gamma_{so}}}$ and $\Psi_1^{1'} = \frac{p}{\rho^{\gamma_{eq}}}$		$\Psi_{ns+nv_1+2}^1 = \frac{p}{\rho^{\gamma_{so}}}$ and $\Psi_{ns+nv_1+2}^{1'} = \frac{p}{\rho^{\gamma_{eq}}}$
$\Psi_{i+1}^1 = Y_i \; i = 1, ns$	$\Psi_1^2 = u$	$\Psi_{i+1}^{ns+nv+2} = Y_i \; i = 1, ns$
$\Psi_{ns+i+1}^1 = \frac{E_{vib}^i}{\rho} \;\; i = 1, nv_1$		$\Psi_{ns+i+1}^{ns+nv+2} = \frac{E_{vib}^i}{\rho} \;\; i = 1, nv_1$
$\Psi_{ns+nv_1+2}^1 = u + \frac{2}{\gamma_{so}-1}a$	$\Psi_2^2 = p$	$\Psi_{ns+nv_1+2}^{ns+nv_1} = u + \frac{2}{\gamma_{so}-1}a$

Table 3.3

3.4 Determination of the intermediate states

In this section, we show how to use these approximate Riemann invariants to get the intermediate states $U_{1/3}$ and $U_{2/3}$:

- For the wave $u-a$:

$$\left(\frac{p_L}{\rho_L}\right)^{\gamma_{soL}} = \left(\frac{p_{1/3}}{\rho_{1/3}}\right)^{\gamma_{so1/3}}$$

$$Y_i^L = Y_i^{1/3} \;\; i = 1, ns$$

$$\frac{E_{vib}^i{}_L}{\rho_L} = \frac{E_{vib}^i{}_{1/3}}{\rho_{1/3}} \;\; i = 1, nv_1$$

$$u_L + \frac{2}{\gamma_{soL}-1}a_L = u_{1/3} + \frac{2}{\gamma_{soL}-1}a_{1/3}$$

- For the wave $u+a$:

$$\left(\frac{p_R}{\rho_R}\right)^{\gamma_{soR}} = \left(\frac{p_{2/3}}{\rho_{2/3}}\right)^{\gamma_{soR}}$$

$$Y_i^L = Y_i^{2/3} \;\; i = 1, ns$$

$$\frac{E_{vib}^i{}_R}{\rho_R} = \frac{E_{vib}^i{}_{2/3}}{\rho_{2/3}} \;\; i = 1, nv_1$$

$$u_R - \frac{2}{\gamma_{soR}-1}a_R = u_{2/3} - \frac{2}{\gamma_{soL}-1}a_{2/3}$$

- through the contact discontinuity :

$$u_{1/3} = u_{2/3} \qquad p_{1/3} = p_{2/3}$$

Then, all the intermediate variables can be expressed by mean of the pressure $p = p_{1/3} = p_{2/3}$ and this leads to the equation :

$$\frac{a_L}{\gamma_{soL}-1}\left[\frac{p}{p_L}\right]^{\frac{\gamma_{soL}-1}{2\gamma_{soL}}} + \frac{a_R}{\gamma_{soR}-1}\left[\frac{p}{p_R}\right]^{\frac{\gamma_{soR}-1}{2\gamma_{soR}}} = \frac{1}{2}(u_L - u_R) + \frac{a_L}{\gamma_{soL}-1} + \frac{a_R}{\gamma_{soR}-1} \tag{3.14}$$

This non linear equation is first preconditioned and the modified equation is solved by Newton iterations. The convergence is reached, in general, after 2 or 3 iterations. This technique have been developed in [19] and is recalled in the next paragraph.

Once this is done, we have the values of the partial densities, velocity, pressure. We need the internal energy for computing the fluxes. This can be achieved by mean of equation (3.11)

The sonic points, if they exist, are obtained with the approximate Riemann invariant as for the classical technique.

Remark : The internal energy and the pressure given by equations (3.11-3.12) are not, in general, consistent. So, the intermediate states $U_{1/3}$ and $U_{2/3}$ are "pseudo" intermediate states.

Discussion of equation 3.14 Equation (3.14) can be written as :

$$f(p) = ap^{\alpha} + bp^{\beta} - c \tag{3.15}$$

with suitable constants a, b, c, α and β. Function f is monotone increasing, concave and equation (3.15) has an unique solution if and only if $c \geq 0$. Equation (3.15) will be solved by Newton iterations :

$$p_{n+1} = p_n - \frac{f(p_n)}{f'(p_n)}$$

but the method can lead to negative values of p if the initial guess p_0 is very big because :

$$\frac{f(p_n)}{f'(p_n)} \simeq \frac{p}{\max(\alpha,\beta)}$$

The idea is to make a change of variable $z = x^{\xi}$ where $\xi = \max(\alpha, \beta)$ and to solve

$$g(z) = z + \frac{B}{A}z^{\eta} - \frac{c}{A} \tag{3.16}$$

where

$$\begin{cases} A = \frac{1}{2}\left[(1 - \text{sign}(\alpha - \beta)\right] a + \frac{1}{2}\left[1 + \text{sign}(\beta - \alpha)\right] b \\ B = \frac{1}{2}\left[(1 - \text{sign}(\alpha - \beta)\right] b + \frac{1}{2}\left[1 + \text{sign}(\beta - \alpha)\right] a \\ \eta = \frac{\min(\alpha,\beta)}{\max(\alpha,\beta)} \leq 1 \end{cases}$$

Function g is much easier to inverse than f : g is monotone increasing, concave as f but its derivative is *always* greater than 1 contrarily to f. The convergence of the Newton iterations is guaranteed if the initial guess is less than the zero ν of g.

One can localize ν : it lies between the zero of functions f_1 and f_2 which are defined by :

$$f_1(p) = (a+b)p^\alpha - c$$

$$f_2(p) = (a+b)p^\beta - c$$

We will usually start the Newton iteration with the smallest of the roots of f_1 and f_2. The convergence will usually be reached with two or three iterations.

3.5 A property of the numerical flux

In the kind of mixture of gas we study here, we may have linear relations between the mass fractions of the various components. For the example of air, these relations means that the proportion of number of moles of oxygen versus that of nitrogen is constant.

This can be formalized in the following way : we consider two linear forms : $\Psi_1(W) = \sum_{i=1,ns} a_i\rho_i$ and $\Psi_2(W) = \sum_{i=1,ns} b_i\rho_i$. We assume that the admissible states lies in the affine space which equation is :

$$\alpha\Psi_1(W) = \beta\Psi_2(W) \tag{3.17}$$

where α and β are constant.

We now consider the first order finite volume scheme which numerical flux is Osher's :

$$W_i^{n+1} = W_i^n - \nu_i\left[\mathcal{F}_{i+1/2}^n - \mathcal{F}_{i-1/2}^n\right] \tag{3.18}$$

In equation (3.18), ν_i stands for the ratio of the time step and mesh size at node x_i. For sake of clarity, the integral part in the Osher's flux be denoted $d(W_i^n, W_{i+1}^n)$ or $d_{i+1/2}$.

We have to show that if relation (3.17) is true at iteration n, then it is true at iteration $n+1$. Since the linear forms Ψ_1 and Ψ_2 are linear and since

$$\Psi_1(F(W_i^n) = \Psi_2(W_i^n)u \quad \Psi_1(F(W_i^n) = \Psi_2(W_i^n)u,$$

we only have to show that

$$\alpha\Psi_1(d_{i+1/2} - d_{i-1/2}) = \beta\Psi_2(d_{i+1/2} - d_{i-1/2}) \tag{3.19}$$

In Section 3.2, we have noticed that the numerical dissipation $d(W_i^n, W_{i+1}^n)$ is a linear combination of the states W_i, W_{i+1}, the pseudo states $U_{1/3}$, $U_{2/3}$ and pseudo sonic states. The coefficients in these linear combinations are independent of the partial densities The partial densities of the pseudo states are :

$$\rho_i^{1/3} = G_L(p,\rho)\rho_L \quad \rho_i^{2/3} = G_R(p,\rho)\rho_R$$

where the terms G_L and G_R do not depend on the partial densities. It is then obvious that for any l :

$$\alpha\Psi_1(d_{l+1/2}) = \beta\Psi_2(d_{l+1/2})$$

This proves equation (3.19).

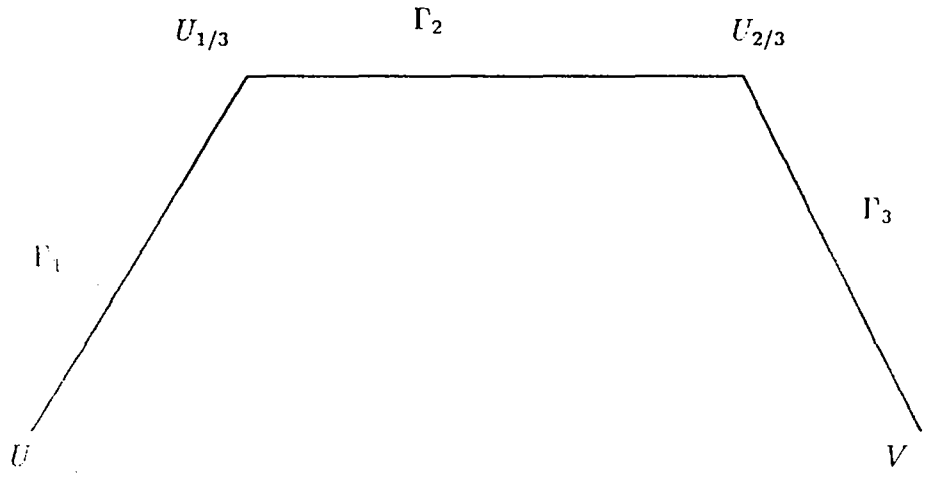

Figure 3.1: Pathes and intermediate states

Chapter 4

Numerical experiments

This new solver have been tested on 1-D and 2-D cases. They are solved with assumption of thermal equilibrium which is the most unfavourable because of the assumptions we have made in section 3.3.

The scheme is based on a finite volume formulation. It is explicit for the convective terms and implicit for the source terms introduced by the dissociation-relaxation processes and the vibrational relaxation. The calculation uses the classical MUSCL method [27] in the 1D cases . The bidimensional calculations are done by using a finite element/finite volume/first order approximation (see [15] for details).

We have used the property of conservativity of the proportion of species to reduce the size of the linear systems to solve at each time steps. For example, in 1D applications, the original system is a 5 one. Since we have two linear linear combination of species, this implies the same relation on the source term. So the effective system to solve is only 3. The same idea is applied in case of vibrational relaxation.

4.1 1D test cases

We have run this new solver on numerous cases (for example those taken from [13]). We have chosen to report the results we have obtained on the one which seems to be the most difficult. It is taken from Suresh et al [2] or [14]. It is defined as follows :

- Left : $p = 100$ atm, $T = 9000$ K and $u = 0$
- Right : $p = 1$ atm, $T = 300$ K, $u = 0$.

There is a large jump in pressure and temperature : the composition of the mixture are completely different and so the vibrational part of the internal energy. This difficult test case has been chosen in order to test the assumptions made in section 3.3. The calculations are second order and use the limitation procedure on the characteristic variables. We use 201 grid points.

Frozen case In a first experience, we intend to test this solver without any chemistry source terms. The calculations have been performed with a CFL number of 0.95.

On Figure 4.1, we have plotted the two "gamma" which are used in the computation of the intermediate states. If no equilibrium vibrational effects were present, they would be equal and the approximate Osher solver would be an exact one. We can see that

their behaviour is also different : the sonic gamma is constant in the expansion wave when the equivalent gamma $(1 + \frac{p}{\epsilon_T})$ is not.

On Figure 4.2, we have plotted the mass fraction distributions. They are constant except in the contact discontinuity ($x \simeq 0.85$) as it should be.

On Figures 4.5, 4.6, 4.7, 4.8 and 4.9 where we have plotted the Mach number, the pressure, the density, the temperature and the velocity, we can see a small overshoot (or undershoot) at the end of the expansion wave. Even in the perfect gas case, one can see that default because of the strength of the expansion wave. We insist on the fact that it is neither a consequence of the approximation we have made here nor a consequence of the second order extension of the scheme.

The pressure and the velocity remains constant in the contact discontinuity (Figures 4.6 and 4.9).

We have also plotted the specific entropy on Figure 4.3 which expression in this particular case is [9] :

$$\begin{aligned} & s = \sum_{i=1}^{ns} Y_i c_{v_i} log(p) - c_{p_i} log(\rho) + \sum_{i=1}^{ns} \Phi_i(T) \\ & \text{where } \Phi_i(T) = \int \frac{d}{dT} E^i_{vib} \frac{dT}{T^2} \end{aligned} \tag{4.1}$$

The integrals in equation (4.1) can be expressed by usual functions.

The specific entropy remains constant in the expansion wave as it should be. We have also tried to represent the evolution of the other Riemann invariants. To do this, we have plotted on Figure 4.4 approximations (by finite differences) of the logarithm of

$$\Gamma_- = \frac{\rho}{a}\frac{du}{d\rho} + 1 \quad \text{and} \quad \Gamma_+ = \frac{\rho}{a}\frac{du}{d\rho} - 1$$

An expansion/compression wave can be parametrized by the density, so, when Γ_+ or Γ_- is null, we have an expansion/compression wave associated with $u - a$ for Γ_+ (resp. $u + a$ for (Γ_-). Moreover, when one among Γ_+ or Γ_- is null, the other one takes the value ± 2. We can see on Figure 4.4 that $\frac{\rho}{a}\frac{du}{d\rho} + 1$ is a good approximation of 0 in the expansion wave (from $x \simeq 0.2$ to $x \simeq 0.5$).

Comparison with an extension of Roe's Riemann solver The Mach number and the pressure are plotted on Figures 4.10 and 4.11. These results are obtained by the same scheme with the extension of Roe's Riemann solver derived for thermally equilibrium flows in Abgrall [3] instead of the present version of Osher's. As we can see, the results are nearly the same. However, we must notice that the Roe's calculations needs an entropy fix (Harten's [26]). If this correction is not used, the computation diverges whatever be the CFL number. This demonstrates the robustness of the algorithm.

Test with chemistry source terms On Figures 4.12 to 4.14, we have plotted the same variables than previously but with Park's model as chemistry source term. As we can see, the addition of chemical source terms does not alter the quality of the results. The methodology can easily handle more complicated situations.

On the mass fractions (4.13), entropy (4.14) and temperature (4.18) plots, we can see the differences on both computations. We can see a production of NO in the contact

discontinuity. This explains the small wiggles on the velocity (4.19) and pressure (4.16) at this location : the ratio of specific heat of different species are different (1.4 or 1.66), at the contact discontinuity, the dominant species are N_2, O, O_2 and NO. Since the numerical thickness of this discontinuity is not zero, this induce wiggles on the pressure and then on the velocity. This phenomena would also be present if we had an exact solver at our disposal (see [20] and [7]).

4.2 2D Test case

We have tested our solver on a test case defined for the Hypersonic Workshop for reentry problem which held in Antibes, (France) in January 1990 [1].

The calculation is done on a double ellipse with semi axis of 60 cm. The conditions are defined at 75 km high and are

- Pressure : $P = 2.52$ Pa
- Temperature : $T = 204.3K$

We assume thermal equilibrium. The calculation is done at $\mathcal{M}_\infty = 25$ and the incidence is 30^o. Some results are displayed on Figures 4.20 to 4.22. They include Mach number, Temperature and pressure coefficient lines. The results compare very well to those obtained by Botta et al. [18].

Chapter 5

Conclusion

We have presented here an extension of Osher's Riemann solver. The numerical test we have performed show the robustness of this new solver. They also show that the properties of the Osher's splitting (smoothness and physical shocks) are valid despite the assumptions we have made. In particular no entropy fix is needed to capture shocks. The same techniques can also be used for more complex situations such as, for example, ionized gas flows.

In conclusion, this extension give satisfactory results in the applications. The accuracy of the spatial approximation may be increased by an extension to second order. The convergence to steady state may be accelerated by using an implicit δ-scheme for example. These two points are currently under study.

Acknowledgements : We wish to thanks our colleague J.A. Désideri for providing us with the mesh used in Section 4.2.

Bibliography

[1] J.A. Désideri, J. Periaux. Workshop on Hypersonic Flows for Reentry Problems, List of Test Problems. INRIA-GAMNI. December 1988.

[2] A. Suresh, M. Liou. The Osher Scheme for Real Gases. AIAA 90-0397.

[3] R. Abgrall. *An Extension of Roe's Upwind Scheme to Algebraic Equilibrium Real Gas Models.* Technical Report 1189, INRIA, March 1990.

[4] R. Abgrall. *Preliminary Results on the Extension of Roe's Riemann Solver to Non Equilibrium Flows.* Technical Report 987, INRIA, March 1989.

[5] B. Grossman, P. Cinnella. *Flux-split Algorithms for Flows with Non-Equilibrium Chemistry and Vibrational Relaxation.* Technical Report 88-08-03, ICAM, 1988.

[6] B. Grossman, R.W. Walters. An Analysis of Flux-Split Algorithms for Euler's Equation Real Gases. In *8th Computational Fluid Dynamics Conference*, page 177, AIAA, 1987.

[7] B. Larrouturou and L. Fezoui. *On the Equation of Multi-Component Perfect or Real Gas Inviscid Flow.* Carasso, Charrier, Hanouzet and Joly, Springer-Verlag, 1989.

[8] C. Park. On the Convergence of Chemically Reacting Flows. AIAA paper No 85-0247 , 23rd Aerospace Sciences Meeting, Reno, Nevada, January, 14-17 1985.

[9] Anne Decamps. Private communication.

[10] F. Dubois. *Programm TEBALDI - Evaluation du flux d'Osher pour l'air à l'équilibre chimique.* Technical Report 104/88, Aérospatiale, April 1989.

[11] P. Glaister. An Approximate Linearised Riemann Solver for the Euler Equations for Real Gases. *Journal of Computational Physics*, 74, 1988.

[12] J.L Montagné. *Recherche Fondementales sur les Méthodes numériques pour les écoulements hypersoniques.* Technical Report 16/1123 AY 218A, ONERA, Janvier 1988.

[13] H.C. Yee and M. Vinokur J.L. Montagné. *Comparative Study of High-Resolution Shock-Capturing Schemes for Real Gas.* Technical Report TM-86839, NASA, July 1987.

[14] J.S. Shuen, B. Van Leer and M.S. Liou. A Detailed Analysis of Inviscid Flux Splitting Algorithms for Real Gases with Equilibrium of Finite-Rate Chemistry. Internationnal Conference in Numerical Methods, Williamsburg, June 1988.

[15] L. Fezoui, B. Stoufflet. A Class of Implicit Upwind Schemes for Euler Simulations with Unstructured Meshes. *Journal of Computational Physics*, 84(1) pp : 174–206, September 1989.

[16] M. Vinokur, J.L. Montagne. *Generalized Flux-Vector Splitting for an Equilibrium Real Gas.* Technical Report 177513, NASA, December 1988.

[17] M.S. Liou, B. van Leer and J.S. Shuen Splitting of Inviscid Fluxes for Real Gases. *Journal of Comp. Physics*, 87(1) pp : 1–24, March 1990.

[18] N. Botta, M.C Ciccoli, J.A. Desideri, L. Fezoui, N.Glinsky, E. Hettena, C. Olivier. Contribution 36 : Reactive Flows over the Double Ellipse. Workshop on Hypersonics Flows for Reentry Problems.

[19] R. Abgrall, J.L. Montagné. Extension of Osher's Riemann Solver for Mixtures of Perfect Gases and Real Gases. *La Recherche Aerospatiale*, 4(1989-4) pp : 1–13, July-August 1989.

[20] R. Abgrall. Generalization of Roe's Rieman Solver to Mixture of Perfect Gas. *La Recherche Aérospatiale*, 1988.

[21] S. Osher S. Chakravarthy. Numerical Experiments with the Osher Upwind Scheme for the Euler Equations. *AIAA Journal*, 21(9), 1983.

[22] F. Solomon S. Osher. Upwind Difference Scheme for Hyperbolic Systems of Conservation Laws. *Mathematics of Computation*, 38(158) pp : 339–374, April 1982.

[23] M. Vinokur. *Flux Jacobian Matrices and Generalized Roe Average for an Equilibrium Real Gas.* Technical Report 177512, NASA, December 1988.

[24] W.G. Vincenti, C.H Kruger. *Introduction to Physical Gas Dynamics.* R.E. Krieger Publishing Co, Malabar/Florida, 1982.

[25] Yen Liu, M. Vinokur. *Nonequilibrium Flows Computations : I. An analysis of Numerical Formulations of Conservation Laws.* Technical Report 177489, NASA, 1989.

[26] A. Harten and J. Hyman *A Selft-adjusting Grid for the Computation of Weak Solutions of Hyperbolic Conservation Laws.* Report LA9105, Center for Nonlinear Studies, Theoretical Division, Los Alamos National Lab., NM, 1981

[27] B. van Leer. Towards the Ultimate Conservative Difference Scheme, III *Journ. of Comp. Physics*, 23 (1977), pp. 263-275.

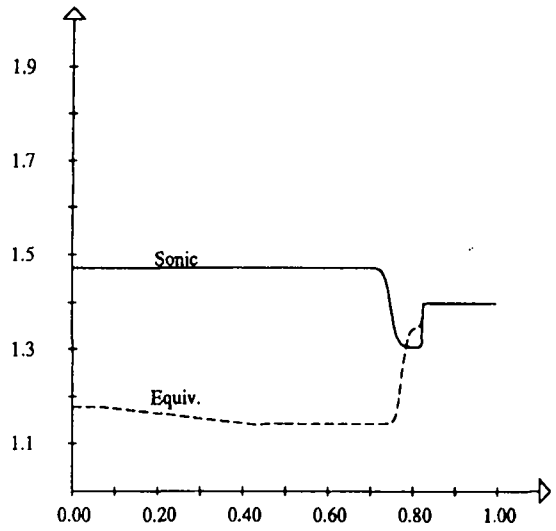

Figure 4.1: Sonic and equivalent gamma , frozen case

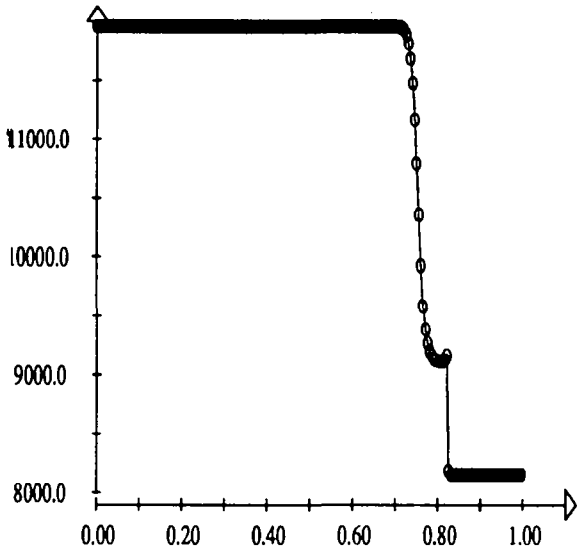

Figure 4.3: Specific entropy, frozen case

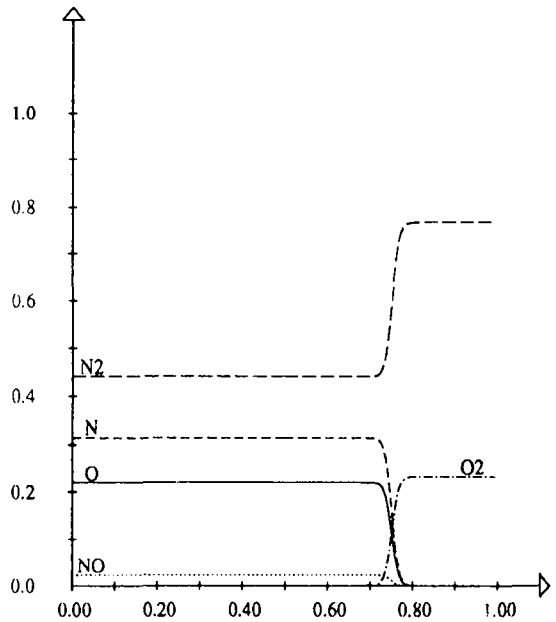

Figure 4.2: Mass fractions, frozen case

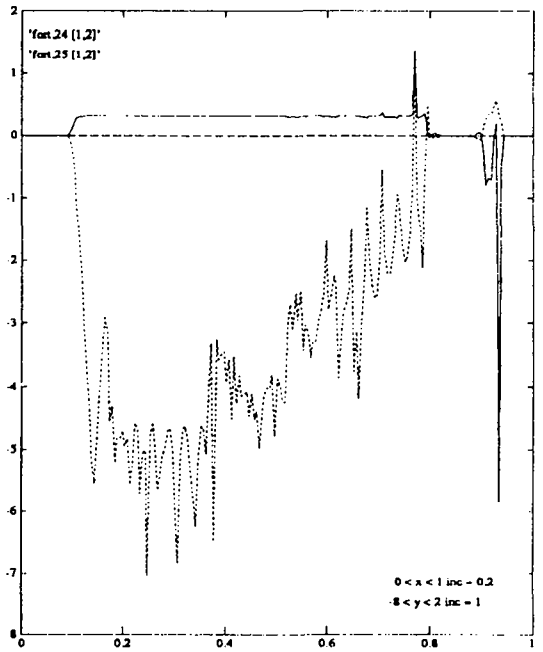

Figure 4.4: Riemann invariants, frozen case

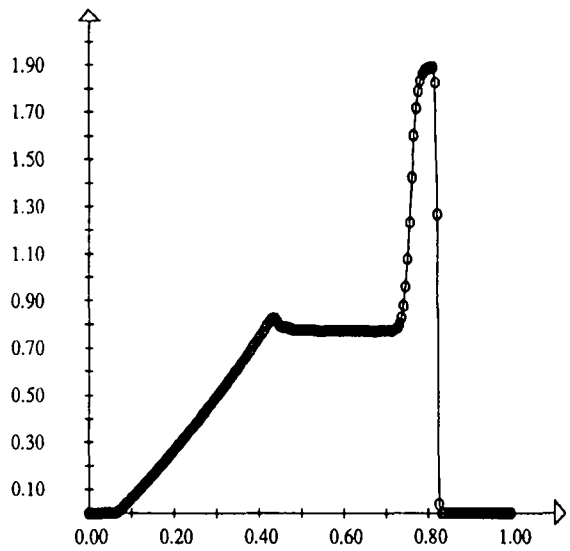

Figure 4.5: Mach Number, frozen case

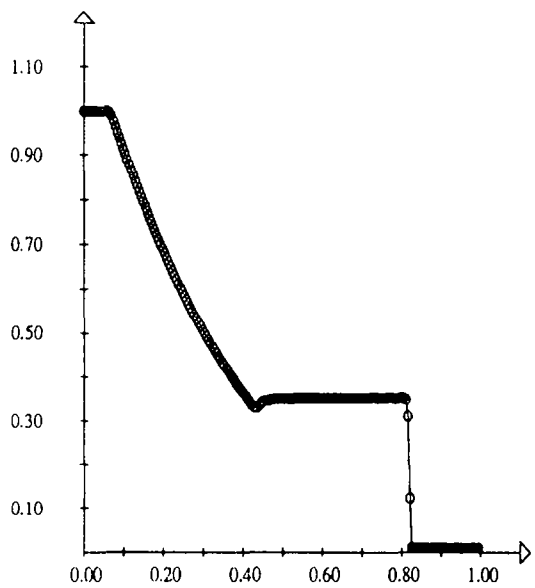

Figure 4.6: Pressure, frozen case

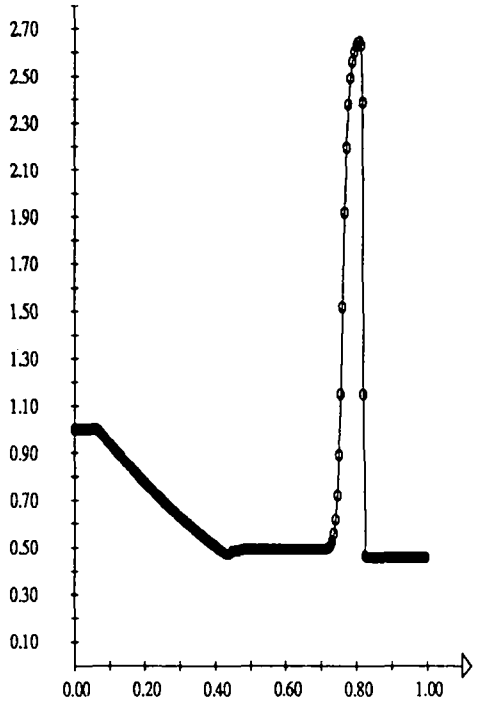

Figure 4.7: Density, frozen case

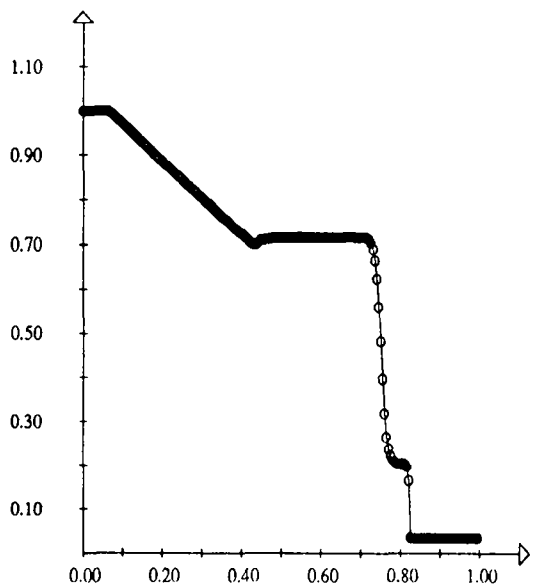

Figure 4.8: Temperature, frozen case

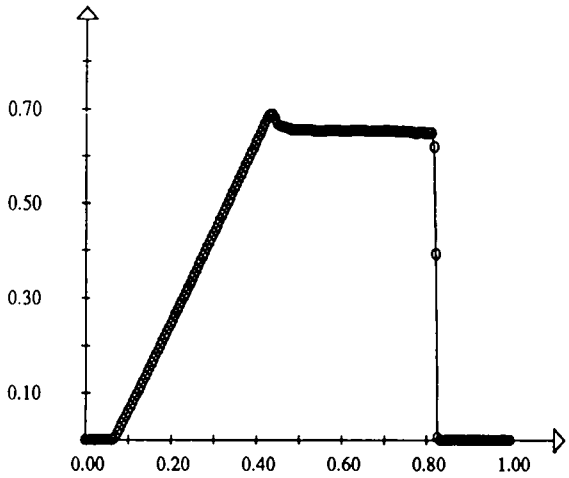

Figure 4.9: Velocity, frozen case

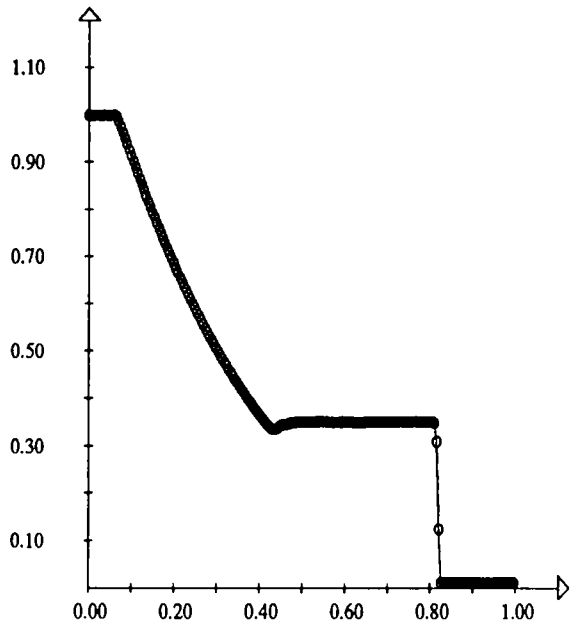

Figure 4.11: Pressure, frozen case and Roe's solver

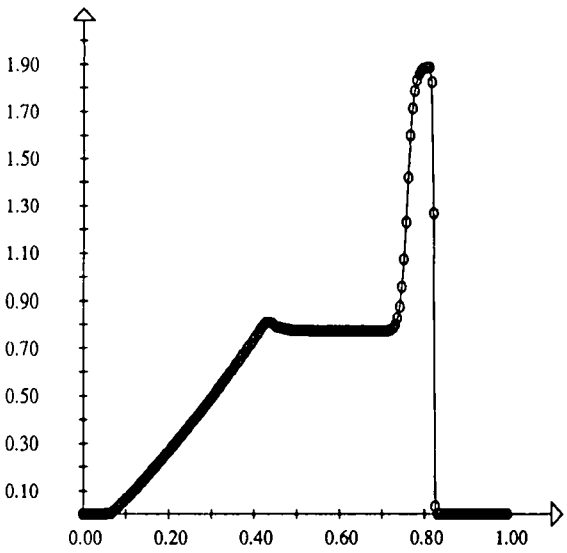

Figure 4.10: Mach number, frozen case and Roe's solver

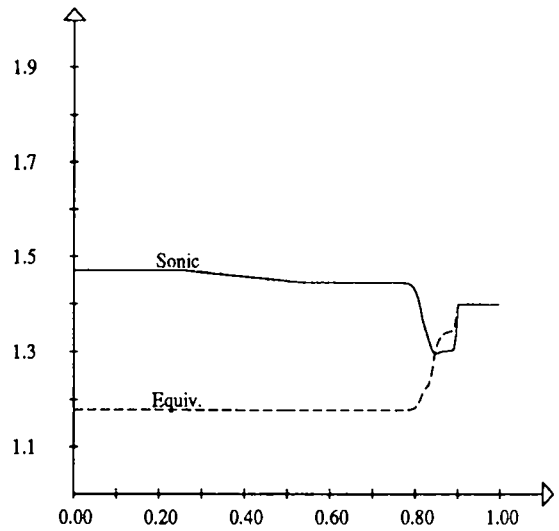

Figure 4.12: Sonic and equivalent gamma , Non equilibrium case

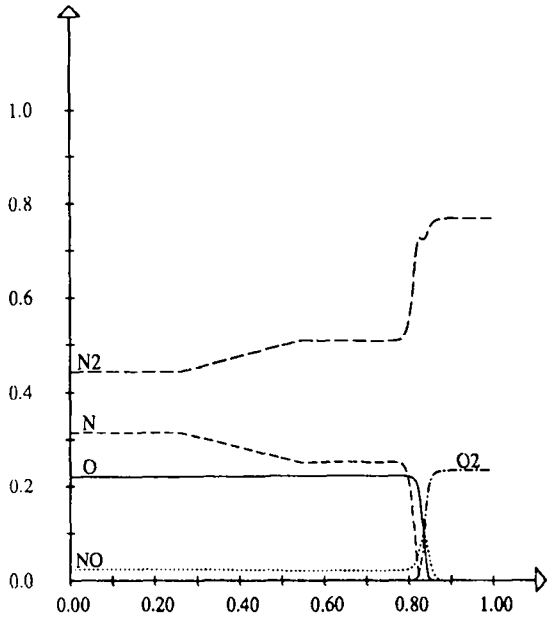

Figure 4.13: Mass fractions, Nonequilibrium case

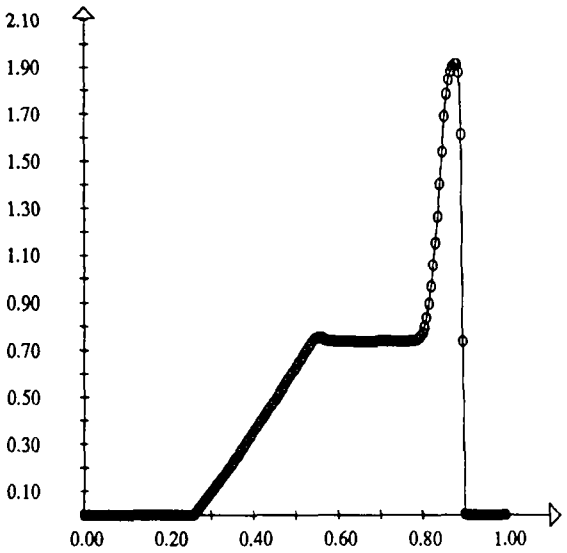

Figure 4.15: Mach Number, Nonequilibrium case

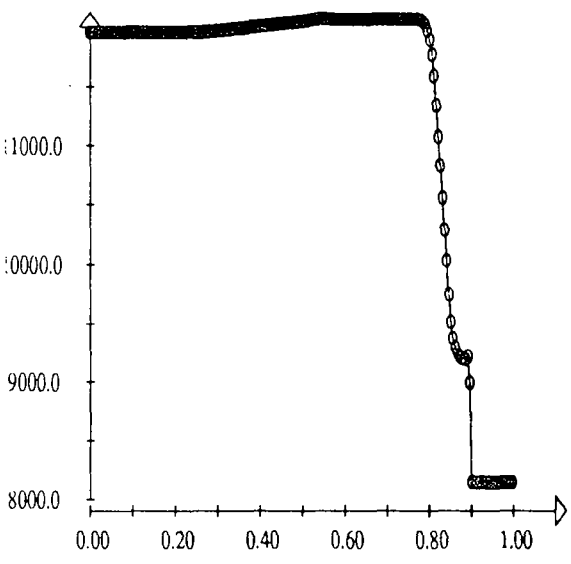

Figure 4.14: Specific entropy, Nonequilibrium case

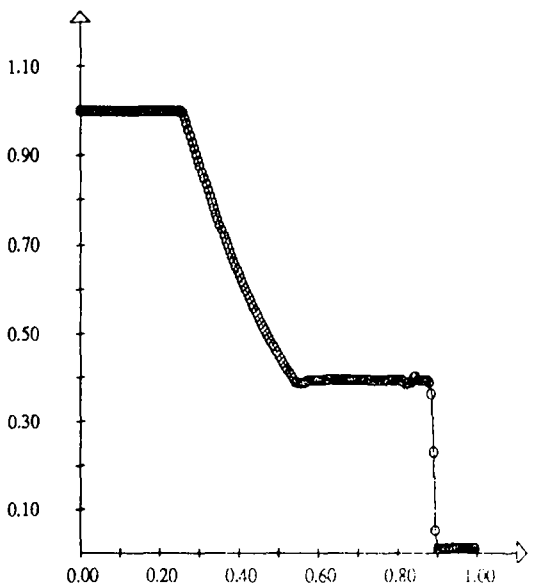

Figure 4.16: Pressure, Nonequilibrium case

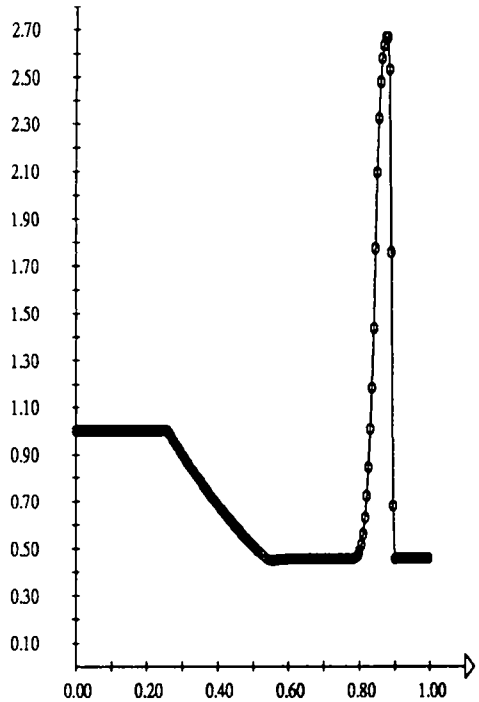

Figure 4.17: Density, Nonequilibrium case

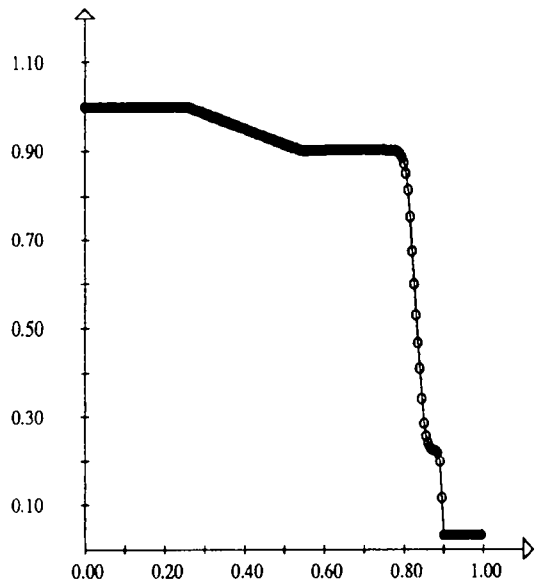

Figure 4.18: Temperature, Nonequilibrium case

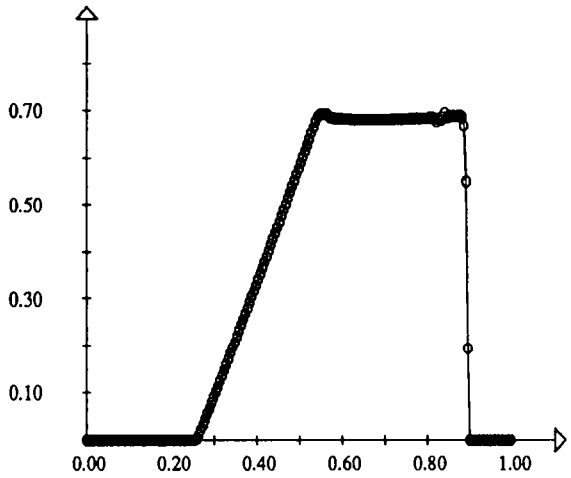

Figure 4.19: Velocity, Nonequilibrium case

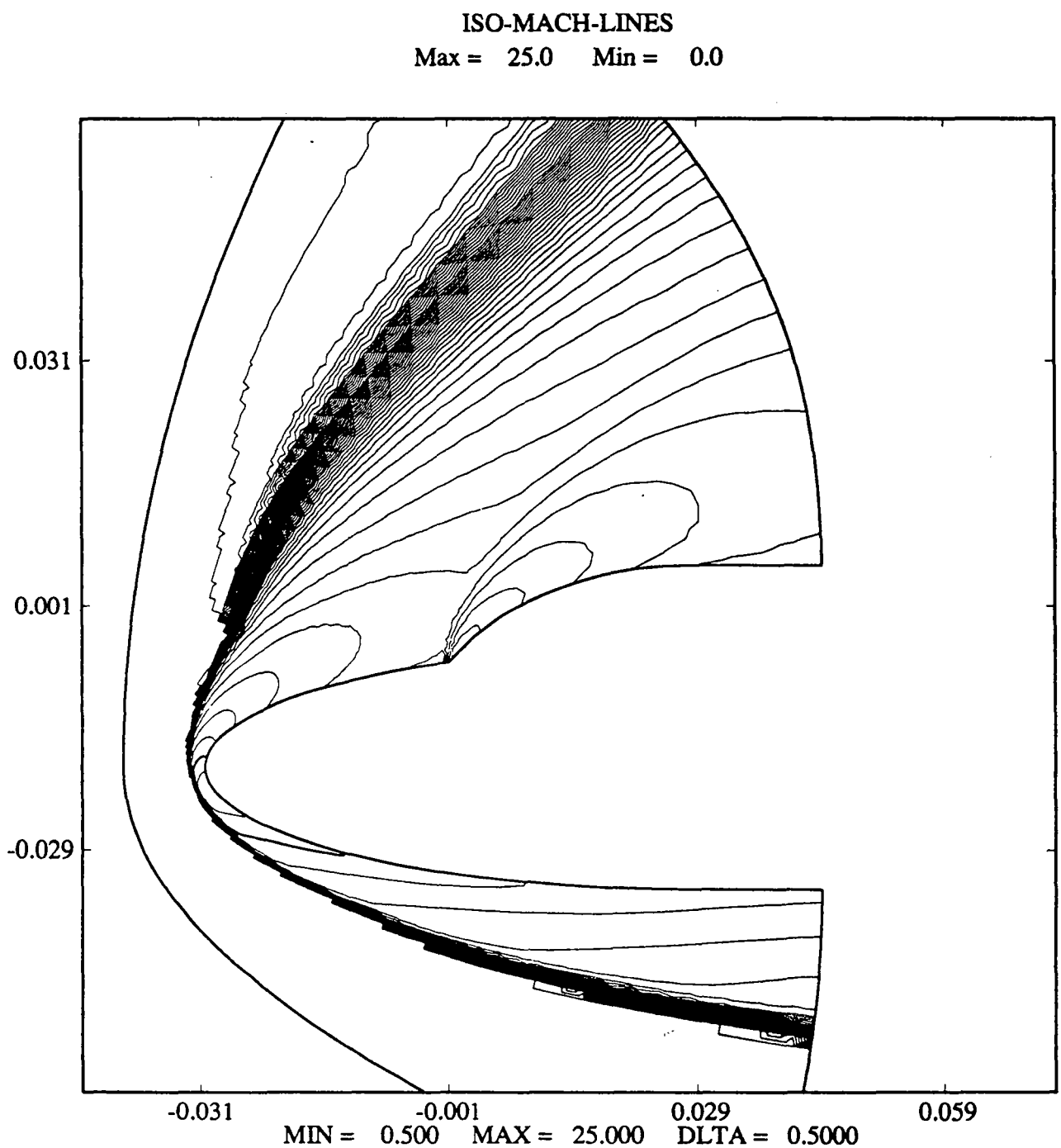

Figure 4.19a : Mach Number, $dM = .5$

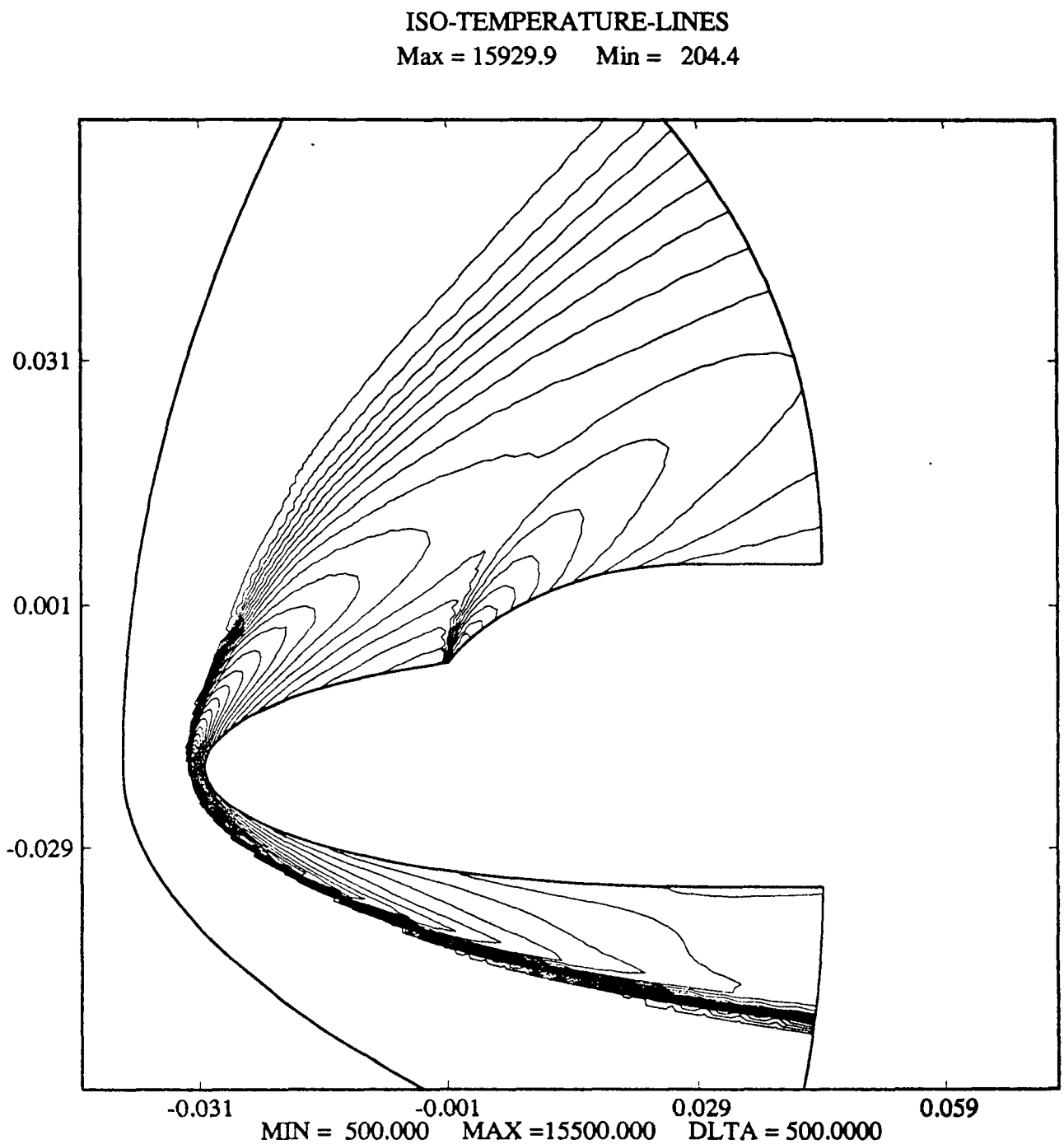

Figure 4.19b : Temperature, Nonequilibrium case, Min=203, Max=15929, $dT = 500$

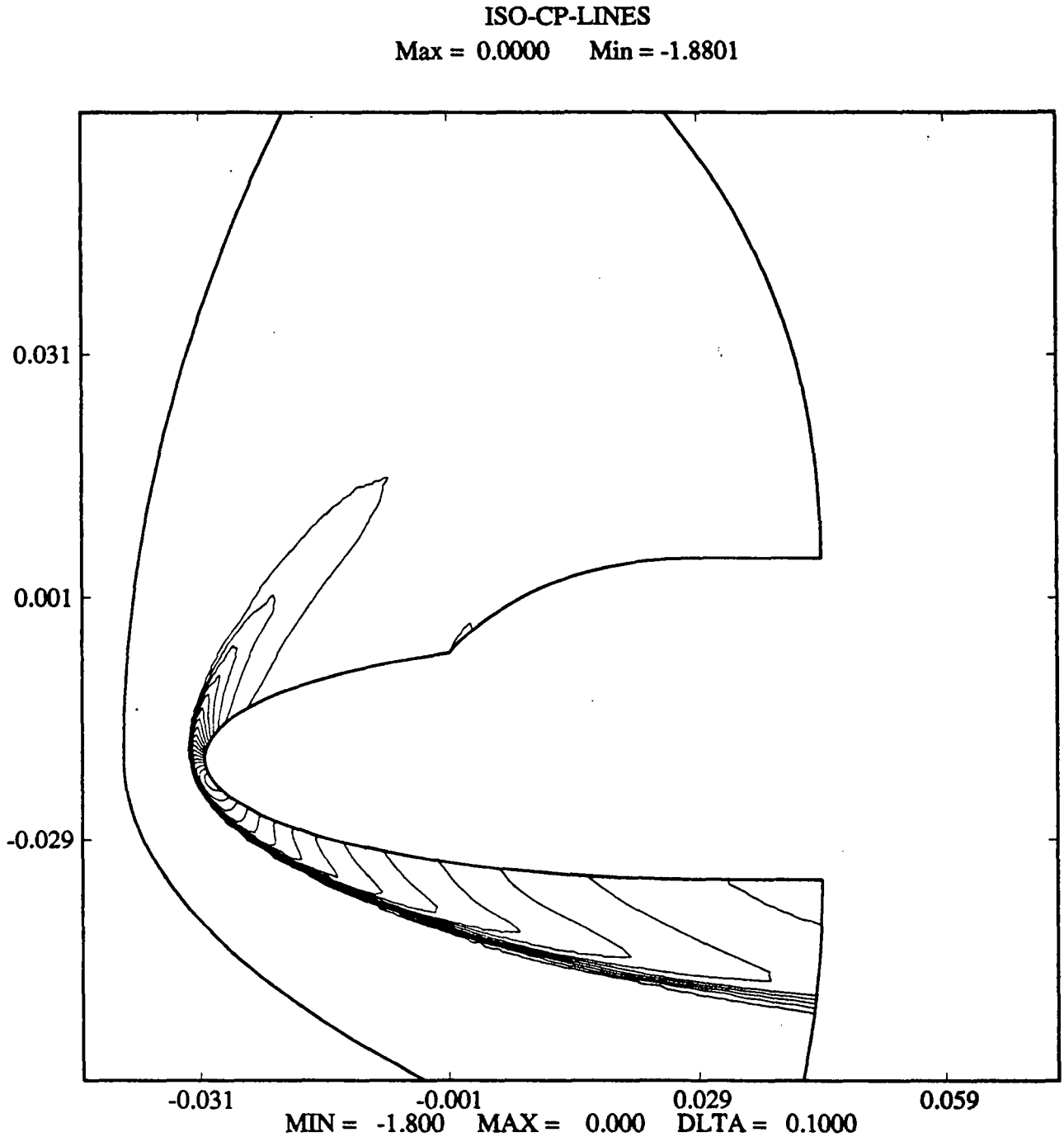

Figure 4.20: Pressure coefficient, min=−1.88, max=0, $dc_p = .1$

Imprimé en France
par
l'Institut National de Recherche en Informatique et en Automatique

ISSN 0249-6399